ACS OMEGA

http://pubs.acs.org/journal/acsodf

Article

Brilliant Nonlinear Optical Response of Ho^{3+} and Yb^{3+} Activated YVO_4 Nanophosphor and Its Conjugation with Fe_3O_4 for Smart Anticounterfeit and Hyperthermia Applications

Ramaswamy Sandeep Perala, Rashmi Joshi, Bheeshma Pratap Singh,* Venkata Nagendra Kumar Putta,* Raghunath Acharya,* and Raghumani Singh Ningthoujam*

Cite This: *ACS Omega* 2021, 6, 19471−19483

Read Online

ACCESS | Metrics & More | Article Recommendations | Supporting Information

ABSTRACT: YVO_4:Ho^{3+}/Yb^{3+} nanophosphors prepared by an effective polyol-mediated route show dual-mode behavior in photoluminescence. Upon 980 nm excitation, the upconversion red emission spectrum exhibits a bright red peak at ∼650 nm, characteristic of the electronic transition of the Ho^{3+} ion *via* involvement of two-photon absorption, which has been confirmed by the power-dependent luminescence study. Moreover, at 300 nm excitation, downconversion emission peaks are observed at 550, 650, and ∼755 nm. The nonradiative resonant energy transfer occurs from the V−O charge transfer band to Ho^{3+} ions, resulting in an improved emission of Ho^{3+} ions. Moreover, polyethylene glycol-coated nanoparticles make it suitable for water dispersibility; and these particles are conjugated with Fe_3O_4 nanoparticles to form magnetic−luminescent hybrid nanoparticles. Highly water-dispersible magnetic−luminescent hybrid material attained the hyperthermia temperature (∼42 °C) under an applied AC magnetic field. The specific absorption rate value is found to be high (138 W/g), which is more than that of pure superparamagnetic Fe_3O_4 nanoparticles. At 300 nm excitation, the high quantum yield value of ∼27% is obtained from YVO_4:Ho^{3+}/Yb^{3+}, which suggests that it is a good phosphor material. By employing the neutron activation analysis technique, it is shown that nanophosphor particles can absorb Au^{3+} up to the ppm level. Interestingly, such nanophosphor also shows the potentiality for anticounterfeiting applications.

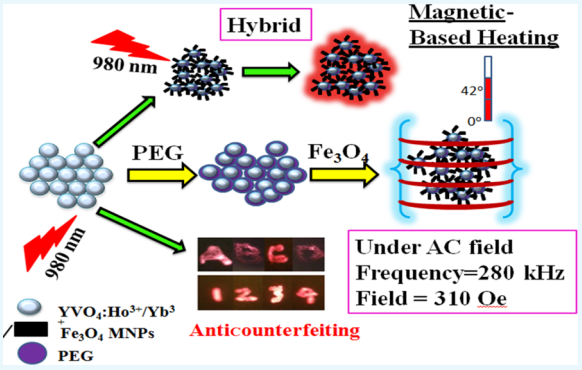

1. INTRODUCTION

Rare-earth (RE)-doped nanocrystals have shown promising applications as compared to pre-existing traditional organic dyes and quantum dots owing to their less toxicity, high penetration depth in biological tissues, longer lifetime of emitting levels, less autofluorescence, and high photostability.[1−4] Recently, RE-doped metal halide perovskites, $Y_2Si_2O_7$ and $Sr_9Al_6O_{18}$ nanocrystals, have been reported.[5−7] However, RE-doped YVO_4 has many advantages as compared to others such as RE-doped metal halide perovskites, $Y_2Si_2O_7$ and $Sr_9Al_6O_{18}$, because the YVO_4 host can become a self-sensitizer in luminescence and also has a low phonon frequency (∼800 cm^{-1}), which reduces the nonradiative decay pathways and promotes the radiative transition pathways significantly.[8]

In addition, YVO_4 nanocrystals have been used as a host for downconversion (DC) luminescent material.[8] This is due to the presence of the allowed transition such as the charge transfer (CT) process of O^{2-} to V^{5+}, which absorbs light from 220 nm to 330 nm with maximum absorption at 300 nm. Upon UV light excitation, it exhibits bluish green emission (350−520 nm) with maximum absorption at 420 nm. On the other hand, RE ions show very weak absorption due to the forbidden transition of f−f as well as self-quenching among them, and consequently, their emission intensity is very weak.[9,10] One of the RE ions having green (550 nm) and red (650 nm) emission is Ho^{3+}, and this ion has absorption peaks at 425 and 455 nm, which fall in the broad emission band of V−O CT. Thus, resonance energy transfer (ET) occurs from VO_4^{3-} ions to Ho^{3+} ions through a nonradiative process, and thereby strong emission from Ho^{3+} ions occurs at 550 and 650 nm.[11−13] Thus, RE ions such as Ho^{3+} and Eu^{3+} ions have been doped into YVO_4 to enhance luminescence intensity.[14−16] Au nanoparticles conjugated with upconversion (UC) nanoparticles $NaYF_4$:Er^{3+}/Yb^{3+} exhibit a strong fluorescence ET or Förster ET mechanism. Here, the absorption band of Au (surface plasmon resonance absorption peak at 542 nm) overlaps with the emission band of Er^{3+}

Received: March 24, 2021
Accepted: June 30, 2021
Published: July 19, 2021

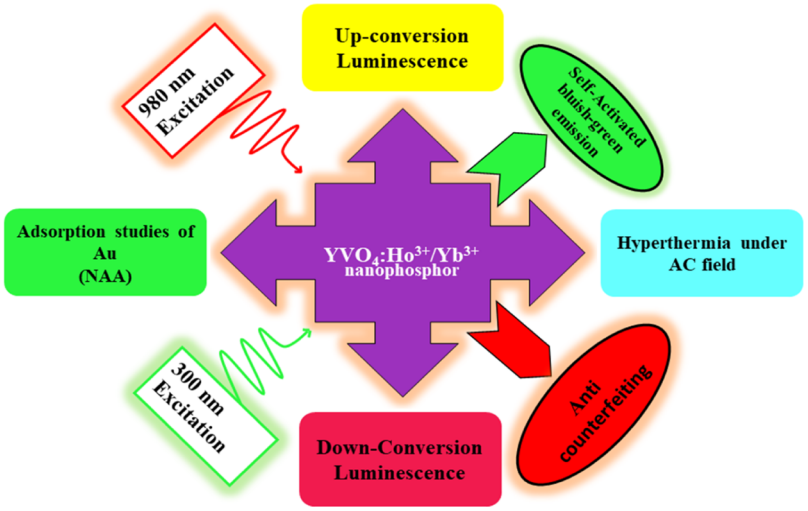

Figure 1. Schematic diagram representing the various applications of YVO_4:Ho^{3+}/Yb^{3+} and its hybrid with Fe_3O_4.

(emission peak at 540 nm).[17] Thus, such UC nanoparticles find many applications.[18,19] In this way, the required heat for hyperthermia treatment of cancer can be generated through the photothermal process. The emission peaks of the Er^{3+} ion are almost the same as those of the Ho^{3+} ion. The intensity ratio of peaks at 550 and 650 nm will be important in biological applications. The variation of the intensity ratio at various excitation wavelengths at 300 nm (V−O CT in DC process), 455 nm (Ho^{3+} in DC process), and 980 nm (UC process) was not much addressed in the literature.

On the other hand, Fe_3O_4 superparamagnetic nanoparticles (SUPs) have been used in many applications due to their high biocompatibility in the area of hyperthermia-based cancer treatment, magnetic resonance imaging contrast agents, carrier for drugs, removal of toxic ions, gene therapy, and so forth.[20−26] In order to trace such SUPs in a living body, it needs to tag with either radioisotopes or luminescence molecules or particles. Our group reported that the Fe_3O_4 SUP showed high absorption capacity toward the RE ions having a radioactivity of a short lifetime (2−64 h) such as ^{90}Y, ^{153}Sm, ^{166}Ho, ^{169}Er, and ^{177}Lu, which emitted β-rays.[21] β-rays are useful for the treatment of arthritis as well as tracking. A combination of magnetic as well as luminescence nanoparticles (known as hybrid) will provide many potential applications, in which individual magnetic or luminescence particles have limitations. Such a combination was started in 2013 by our group.[24]

The Commission International de I'Eclairage (CIE) 1931 chromaticity program was used to see the color obtained from DC spectra. However, unacceptable CIE coordinates (close to x = 0.33 and y = 0.33, white color) were observed for various samples (irrespective of samples) from the UC emission upon excitation at 980 nm. The reason for this was not addressed so far in the literature.[27]

In this work, we have prepared YVO_4:Ho^{3+}/Yb^{3+} nanophosphor *via* an effective polyol-mediated route. Its luminescent behavior has been studied by various excitations at 980 nm (due to Yb^{3+} absorption), 300 nm (indirect V−O charge transfer band, CTB), and 455 nm (due to Ho^{3+} absorption). Its DC, ET efficiency, and UC processes are discussed. The sensing behavior of such particles in Au^{3+} ions has been studied using the neutron activation analysis (NAA) technique. The synthesized nanophosphor material is studied for its anti-counterfeiting applications. The prepared nanohybrid (Fe_3O_4@YVO_4:Ho^{3+}/Yb^{3+}) exhibits the bifunctional properties (*i.e.*, luminescence as well as magnetic) for hyperthermia and bioimaging applications because the luminescence peak arises at 650 nm, which lies in the first biological imaging window (600−900 nm) under 980 nm excitation. The quantum yield study of samples is carried out. Also, the source of errors in the calculation of CIE coordinates of samples from the UC emission spectrum is explained. The zeta potential values of YVO_4:Ho^{3+}/Yb^{3+} are evaluated for potential bioimaging purposes. Figure 1 shows the schematic diagram of dual-mode behavior, that is, DC and UC nanophosphor, anticounterfeit, hyperthermia, and Au^{3+} ion adsorption studies.

2. RESULTS AND DISCUSSION

2.1. XRD Study. Figure S1 shows the XRD pattern of nanophosphor YVO_4: 1 at. % Ho^{3+} and 10 at. % Yb^{3+} (annealed at 900 °C and referred to as YVO_4:Ho^{3+}/Yb^{3+}). The XRD patterns reveal that the diffraction patterns are well matched with standard JCPDF no. 76-1649 (pure YVO_4) of the tetragonal structure. Here, Yb^{3+} (r = 0.985 Å) and Ho^{3+} (r = 1.015 Å) ions got substituted at Y^{3+} (r = 1.019 Å) sites of the YVO_4 lattice because they have similar ionic radii on the basis of coordination number eight, where Y^{3+} ion is surrounded by eight O^{2-} ions.[28]

The nanophosphor exhibits a tetragonal structure with high crystallinity having space group $I4_1/amd$. The lattice parameters for the nanophosphors are calculated using UnitCellWin software. The estimated lattice parameters are a = 7.082 Å, c = 6.219 Å, and unit cell volume V = 312.01 Å^3, which are comparable with those of pure YVO_4 (JCPDF file no. 76-1649) a = 7.123 Å, c = 6.292 Å, and V = 319.23 Å^3. The average crystallite size is calculated to be ∼60 nm.

As shown in Figure S1, the XRD pattern of Fe_3O_4 exhibits the face-centered cubic structure. The lattice parameter is calculated to be a = 8.342 Å and V = 580.52 Å^3. The crystallite size is found to be ∼10 nm. The XRD patterns of both Fe_3O_4@PEG and Fe_3O_4@YVO_4:Ho^{3+}/Yb^{3+} hybrid are also shown in Figure S1. A slight line broadening in the peak is observed in both cases as compared to pure Fe_3O_4 or YVO_4:Ho^{3+}/Yb^{3+}. This suggests that the polyethylene glycol (PEG) coating over the particles affects the crystallite size. In the YVO_4 crystal structure/unit cell, the V^{5+} ion in the $[VO_4]^{3-}$ groups are coordinated tetrahedrally with O^{2-} ions, and the Y^{3+} ion is surrounded by eight O^{2-} ions to

https://doi.org/10.1021/acsomega.1c01572
ACS Omega 2021, 6, 19471−19483

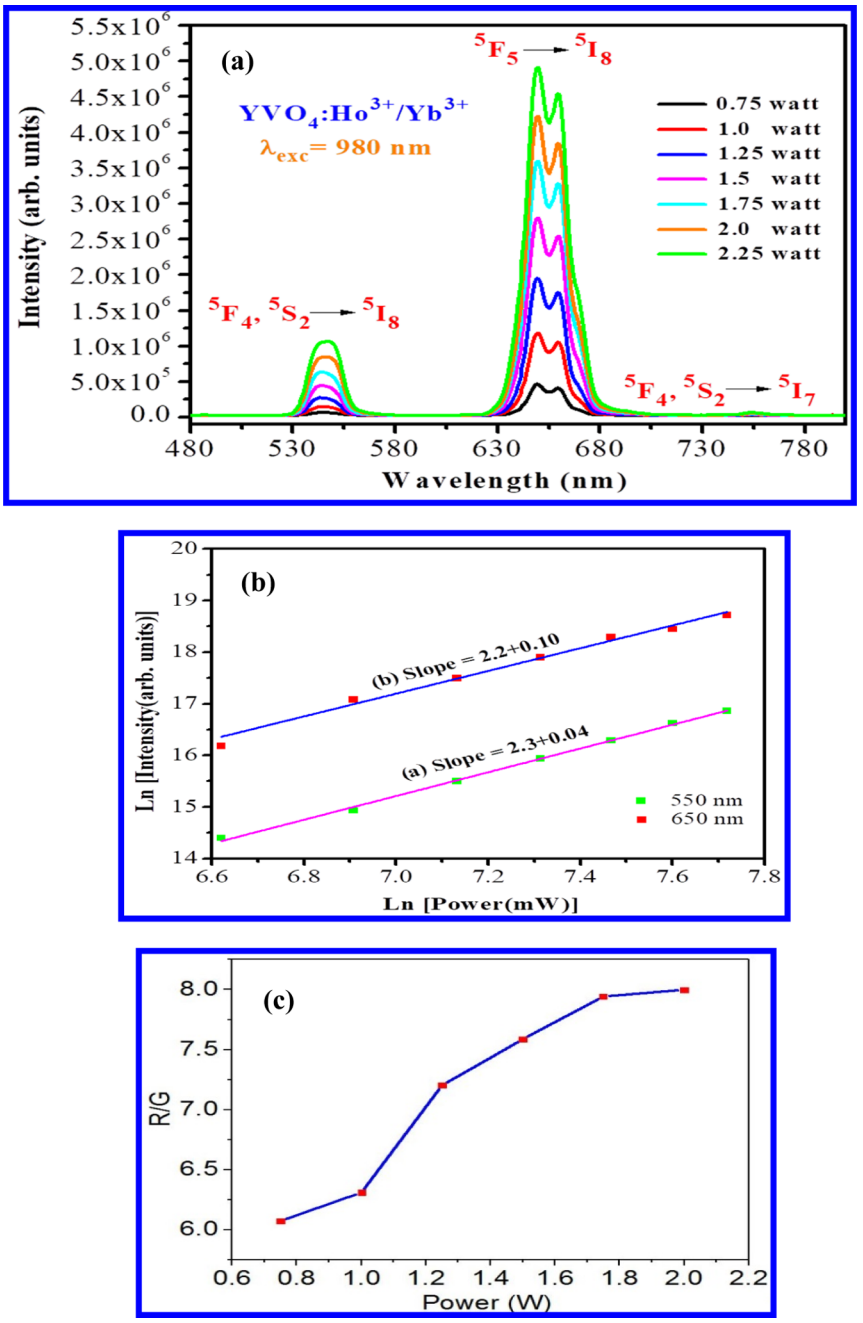

Figure 2. (a) Emission spectra of $YVO_4:Ho^{3+}/Yb^{3+}$ (1 at. % Ho) excited at 980 nm continuous wave (CW) at various powers (P), (b) ln(I) of 550 nm (G) and 650 nm (R) emission vs ln(P), and (c) R/G ratio vs power (R is the red region 650 nm and G is the green region 550 nm). The spot/area of the laser falling on the sample is $2\pi r^2$ (here r = 1 mm).

form a YO_8 dodecahedron. There are two sets of four equal Y−O bond lengths: short and long with point symmetry D_{2d} of Y^{3+}, without inversion. The YVO_4 tetrahedral crystal structure has a space group of $I4_1/amd$. The Y^{3+} ions are substituted by Ho^{3+} and Yb^{3+}, resulting in emissions (discussed later) that are characteristic of D_{2d} point symmetry.[16]

2.2. Thermogravimetric Analysis and Differential Thermal Analysis Studies. Figure S2 shows the thermogravimetric analysis (TGA) and differential thermal analysis (DTA) curves of the as-prepared sample of $YVO_4:Ho^{3+}/Yb^{3+}$ nanophosphor (without annealing at 900 °C). From the TGA curve, there are three stages of mass loss. The first loss of mass (17%) occurs from room temperature to 200 °C corresponding to the removal of adsorbed water on the surface of the particles. The second mass loss occurs over the temperature range from 200 to 550 °C, related to the decomposition of ethylene glycol (EG), which corresponds to approximately 6% of the mass loss. The third mass loss in the temperature range from 550 to 750 °C is due to the removal of carbon that remained in the sample with a mass loss of about 2%. In the DTA curve, these three stages are observed. The first stage is supported by an endothermic peak at 150 °C. The second stage is supported by an exothermic peak at 330 °C. The third stage is supported by an endothermic peak at 700 °C. In this way, pure $YVO_4:Ho^{3+}/Yb^{3+}$ particles without carbon, H_2O, or organic molecule (EG) are obtained above 700 °C.

https://doi.org/10.1021/acsomega.1c01572
ACS Omega 2021, 6, 19471−19483

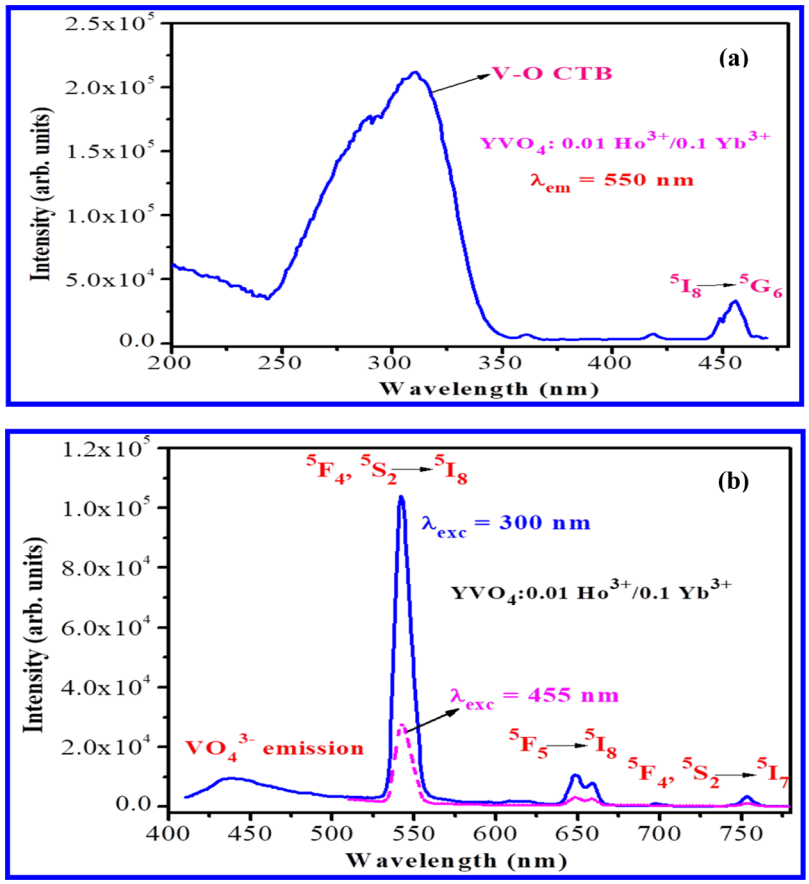

Figure 3. (a) Excitation spectrum of YVO_4:Ho^{3+}/Yb^{3+} (1 at. % Ho) at λ_{em} = 550 nm showing the V−O CTB and the Ho^{3+} peak at 455 nm and (b) its emission spectra at λ_{exc} = 300 and 455 nm showing the peaks due to V−O and Ho^{3+}.

2.3. FTIR Study. Figure S3 shows the FTIR spectra of PEG and as-prepared samples of Fe_3O_4, Fe_3O_4@PEG, YVO_4:Ho^{3+}/Yb^{3+}, and Fe_3O_4@YVO_4:Ho^{3+}/Yb^{3+}. The strong vibrational bands are observed at ∼3430 and ∼1630 cm^{-1} that, respectively, correspond to the stretching and bending vibrations of water (H_2O), which is present on the surface of the nanoparticles.[8,12] The pure PEG shows two bands at ∼1076 cm^{-1} (ν-trans) and ∼1110 cm^{-1} (ν-gauche), which represents the C−O−C stretching vibrations along with CH_2 stretching vibrations (∼2870, ∼2940 cm^{-1}).[8,12] The V−O vibrational band in VO_4^{3-} is observed at 800 cm^{-1}.[8,12] The band at ∼599 cm^{-1} corresponds to Fe−O of Fe_3O_4, and the two bands at ∼1092 and ∼1390 cm^{-1} correspond to S−O, which arises from $FeSO_4{\cdot}7H_2O$ used during the synthesis of Fe_3O_4.[29] The vibrational bands involved in the prepared samples of Fe_3O_4, Fe_3O_4@PEG, YVO_4:Ho^{3+}/Yb^{3+}, and Fe_3O_4@YVO_4:Ho^{3+}/Yb^{3+} are listed in Table S1.

2.4. SEM, EDX, and TEM Studies. Figure S4 shows the SEM image of YVO_4:Ho^{3+}/Yb^{3+} nanophosphor annealed at 900 °C. It shows the irregular shapes of nanoparticles (a large number of spherical shapes along with a small number of rectangular and cuboid shapes). The average size obtained from spherical particles is ∼80 nm. Their elemental compositional images of Y, V, Yb, Ho, and O are shown in Figure S4. Their EDX spectrum is also shown for the elemental compositional analysis (Figure S4), and their elemental compositions are provided in Table S2. However, the peak corresponding to Ho could not be detected due to the presence of a very small concentration, which is under the limit of detection. The theoretical atomic percentages of Y, V, Yb, Ho, and O are 14.8, 16.5, 1.6, 0.2, and 66.6, respectively. The experimental atomic percentages of Y, V, Yb, Ho, and O are 16, 12, 2, 0, and 70, respectively.

For the preparation of TEM imaging for the synthesized samples, the particles are dispersed in ethanol and sonicated for 10 min. One drop of the dispersed part is added over the carbon-coated Cu grid. The TEM image of YVO_4:Ho^{3+}/Yb^{3+} nanoparticles annealed at 900 °C is shown in Figure S5. A mixture of spherical and cuboid shaped particles is observed. The average particle size of the spherical particles is found to be 90 nm.

2.5. Photoluminescence Study. *2.5.1. UC Study.* Upconversion is a nonlinear anti-Stokes shift optical phenomenon in which the low energy input photon is converted into the high energy output photon *via* successive multiphoton absorptions.[30] We have optimized YVO_4:0.01Ho^{3+}/0.1Yb^{3+} nanophosphor from different Ho^{3+} percentages (Ho^{3+} = 1, 3, 5, and 7 at. %) doped YVO_4. The optimized nanophosphor is further examined for UC and DC luminescence studies. Upon 980 nm excitation, the UC emission spectra of YVO_4:Ho^{3+}/Yb^{3+} (1 at. % Ho^{3+} and 10 at. % Yb^{3+}) at different laser powers are shown in Figure 2a. The UC spectra exhibit emission bands at ∼550 nm (green = G), ∼650 nm (red = R), and ∼755 nm, and these bands arise, respectively, due to $^5F_4$, $^5S_2$ → $^5I_8$, $^5F_5$ → $^5I_8$, and $^5F_4$, $^5S_2$ → $^5I_7$ electronic transitions of the Ho^{3+} ion.[15,16] Here, Yb^{3+} ions are acting as sensitizers that has a higher absorption cross section as compared to Ho^{3+} at 980 nm excitation. The absorption cross section of Yb^{3+} is 11.7 × 10^{-21} cm^2 at 980 nm excitation.[19,31−35] The number of photons

https://doi.org/10.1021/acsomega.1c01572
ACS Omega 2021, 6, 19471−19483

involved in the UC is calculated and plotted as shown in Figure 2b. The upconverted emission intensity varies with the laser input power as $I \propto P^n$, where I represents the upconverted intensity, P is the laser input power, and n is the number of photons involved in the upconverted emission bands. The ln(I) versus ln(P) shows slopes of n = 2.3 and 2.2 for G and R, respectively. This suggests that the two-photon process leads to UC emission for both G and R lights. From the spectra (Figure 2c), it is evident that the R/G ratio increases with the laser input power. The focal spot area of the laser beam impinging at the center is governed by $2\pi r^2$ (here r = 1 mm).

2.5.2. DC Study. Downconversion is the process of release of radiative light (E_{em}) of lower energy after absorption of light (E_{exc}), that is, $E_{em} < E_{exc}$. This is referred to as the Stokes shift. Upon UV excitation at 300 nm, the DC emission spectrum of YVO_4:Ho^{3+}/Yb^{3+} (1 at. % Ho) is shown in Figure 3. The green (~550 nm), red (~650 nm), and NIR (~755 nm) emission bands associated with $^5F_4$, $^5S_2 \rightarrow {}^5I_8$, $^5F_5 \rightarrow {}^5I_8$, and $^5F_4$, $^5S_2 \rightarrow {}^5I_7$ electronic transitions of the Ho^{3+} ion, respectively, are observed.[15,16] The emission spectra are monitored at different excitation wavelengths at 260, 290, 300, and 455 nm. Each excitation shows the emission peaks due to Ho^{3+}. Upon direct excitation of Ho^{3+} at 455 nm ($^5I_8 \rightarrow {}^5G_6$), the emission intensity of Ho^{3+} is weaker than that of indirect excitation at 300 nm. This is due to the low absorption cross section of f−f transitions of Ho^{3+}. In the case of excitation at 300 nm, the broad emission band (420−500 nm) associated with VO_4^{3-} in addition to peaks of Ho^{3+} is observed.[8] Due to the allowed transition of the V−O CTB, there is a high absorption cross section at 300 nm. The radiative rate of Ho^{3+} increases as a large number of excited photons of V−O get de-excited, and the excited energy is transferred from V−O to Ho^{3+}. There is an overlapping between the emission band of the V−O CTB and absorption peaks of Ho^{3+}. This is known as the resonance ET from VO_4^{3-} to Ho^{3+}.[8]

The excitation spectrum of YVO_4:Ho^{3+}/Yb^{3+} is shown in Figure 3a after monitoring at a 550 nm emission. A broad peak from 250 to 350 nm with the maximum at 300 nm is observed. This is related to the allowed transition of V−O CTB.[8] The sharp peaks with small intensities due to Ho^{3+} at 360, 425, and 455 nm are observed.[15,16]

In order to see the concentration-dependent luminescence, different amounts of Ho^{3+} are doped into the YVO_4 host at a fixed concentration of Yb^{3+} (10 at. %). Upon excitation at 300 and 455 nm, YVO_4:xHo^{3+}:yYb^{3+} (x at. % = 1, 3, 5, and 7, y at. % = 10) shows emission peaks of Ho^{3+}. The luminescence intensity decreases with the increase of the Ho^{3+} ion beyond 1 at. % (Figure 4). It occurs mainly due to the concentration quenching effect.[25,36]

2.5.3. ET Mechanism. The schematic diagram representing the UC and DC processes involved in YVO_4:Ho^{3+}/Yb^{3+} is shown in Figure 5. The ground state absorption (GSA) of the Yb^{3+} ions can occur at 980 nm CW laser ($^2F_{7/2} \rightarrow {}^2F_{5/2}$) excitation. The GSA process is very weak for Ho^{3+} ($^5I_8 \rightarrow {}^5I_6$) because 980 nm is not matching with the energy gap between the ground state and the excited state. Thus, the incident photons are mostly absorbed by the Yb^{3+} ions and they transfer the energy to nearby Ho^{3+} ions through the ET process known as two- or three-photon absorption, and the various lower lying levels are populated by the nonradiative relaxations from the upper lying levels of Ho^{3+}. The emission peaks at green (~550 nm), red (~650 nm), and NIR (~755 nm) of Ho^{3+} are observed, and these observations were analyzed in the case of the UC process. In the case of the DC process, there is a high absorption

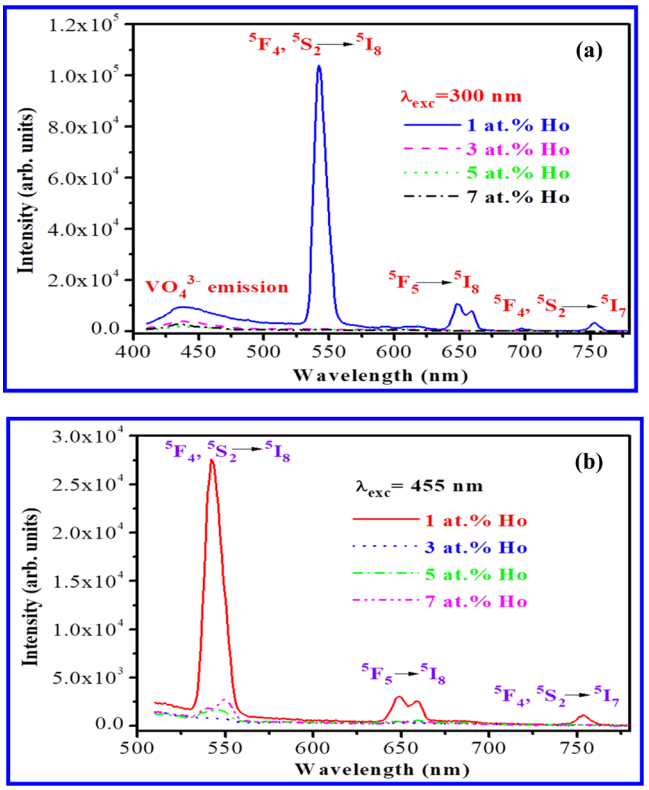

Figure 4. (a) Emission spectra showing the ET from V−O to Ho^{3+} in different percentages of Ho^{3+} in $Y_{1-x-y}VO_4$:xYb^{3+}/yHo^{3+} (x = 0.1, y = 0.01, 0.03, 0.05, and 0.07) at λ_{exc} = 300 nm and (b) their emission spectra at λ_{exc} = 455 nm.

band through the V−O CT at 300 nm and a large number of photons are populated at a higher energy level as excited electrons, and then, depopulation of the excited electrons starts as emitted light in 420−500 nm, which is matching with the absorption band of Ho^{3+} at 455 nm. Because of the ET from the excited level of the V−O CTB to the excited state of Ho^{3+}, an enhanced emission intensity of Ho^{3+} is observed. Upon excitation at 455 nm (direct excitation of Ho^{3+}), the emission intensity of Ho^{3+} is less than that excited at 300 nm by fivefold. It is confirmed that there is an ET from the V−O CTB to Ho^{3+}.[8,16]

The ET from VO_4^{3-} to Ho^{3+} and the quenching mechanism of prepared nanophosphor YVO_4:xHo^{3+}:yYb^{3+} (x = 1, 3, 5, 7, at. % and y = 10 at. %) annealed at 900 °C are examined. The ET may occur by the exchange interaction and electric multipolar interaction. The critical distance (R_c) between VO_4^{3-} and Ho^{3+} ions that depends on both the exchange interaction and multipole−multipole interaction is given by Blasse's equation[32]

$$R_c = 2\left(\sqrt[3]{\frac{3V}{4\pi X_c N}}\right) \quad (1)$$

where V is the volume of the crystallographic unit cell and N is the number of cationic sites that can be occupied by the activator ions per unit cell.

Upon excitation at 300 nm, there occurs an ET from VO_4^{3-} to the Ho^{3+} ion. Further, as the concentration of the xHo^{3+} ion (x = 1, 3, 5, 7, and 10 at. %) increases at fixed yYb^{3+} (y = 10 at. %), the luminescence intensity decreases above >1 at. % of Ho^{3+}. This is due to the concentration quenching effect. Otherwise, the luminescence intensity of Ho^{3+} might increase due to the extent of the ET from VO_4^{3-} to Ho^{3+} (Figure 6). For 1 at. % Ho^{3+}, X_c =

https://doi.org/10.1021/acsomega.1c01572
ACS Omega 2021, 6, 19471−19483

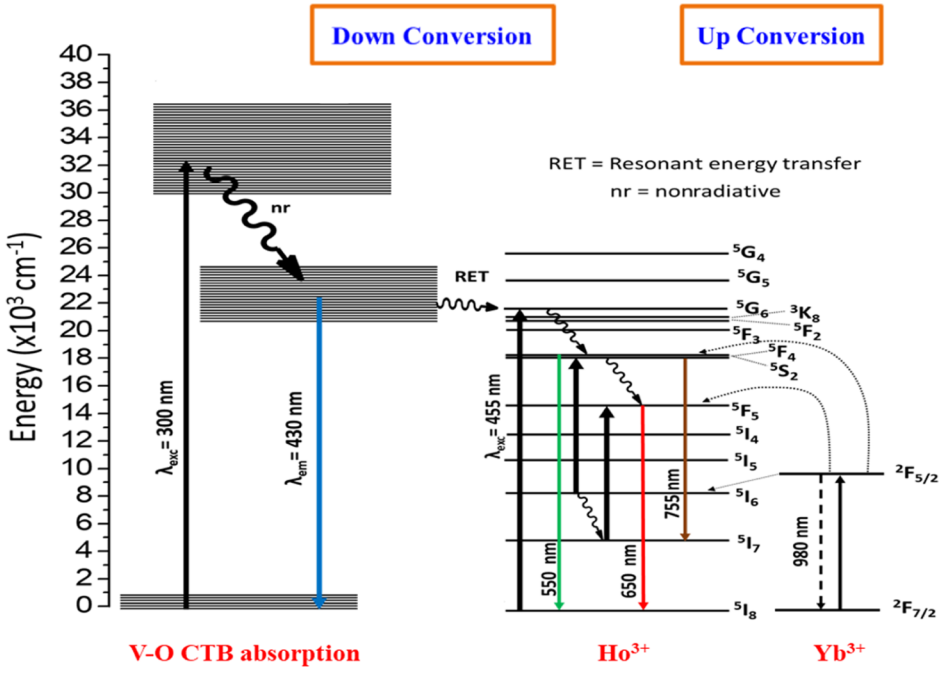

Figure 5. Energy-level diagram of DC and UC of YVO_4:Ho^{3+}/Yb^{3+} nanophosphor.

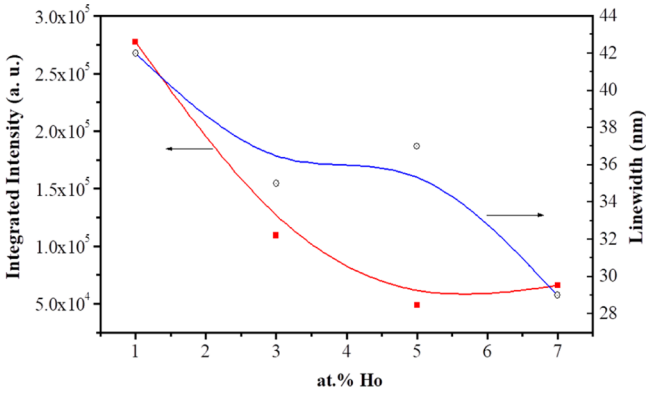

Figure 6. Integrated intensity of the V−O CT peak and the corresponding line width against the concentration of Ho^{3+} in YVO_4:Ho^{3+}/Yb^{3+} nanophosphor.

0.01 (from Ho^{3+}) + 1.0 (VO_4^{3-}) by taking $Y_{(1.0-x-y)}V_{1.0}O_4$. Here, V = 312.00 Å^3 and n = 4 (from Y^{3+} sites) + 4 (from V^{5+} sites) = 8. In the pure tetragonal structure of YVO_4, there are four formula units. After consideration of the abovementioned values, R_c is found to be 4.2 Å.

In the case of excitation at 455 nm, there is an ET among Ho^{3+} ions. Thus, above 1 at. % Ho^{3+}, the intensity of Ho^{3+} decreases with the increase of Ho^{3+}. For 1 at. % Ho^{3+}, X_c = 0.01 (from Ho^{3+}) by taking $Y_{(1.0-x-y)}V_{1.0}O_4$. Here, V = 312.00 Å^3 and n = 4 (from Y^{3+} sites). After consideration of the abovementioned values, R_c is found to be 24.6 Å.

2.5.4. Decay Study. The photoluminescence decay of the $^5F_5$ level (550 nm emission) of the Ho^{3+} ion in YVO_4:0.01% Ho^{3+}/0.1% Yb^{3+} under the excitation of 455 nm is shown in Figure 7a. It is fitted with the monoexponential decay equation[9]

$$I = I_0 \exp\left(\frac{-t}{\tau}\right) \quad (2)$$

where I is the intensity at time t, I_0 is the initial intensity at time t = 0, and τ is the lifetime of the emitting level. The lifetime of YVO_4:0.01% Ho^{3+}/0.1% Yb^{3+} nanophosphor is found to be ∼16 μs.

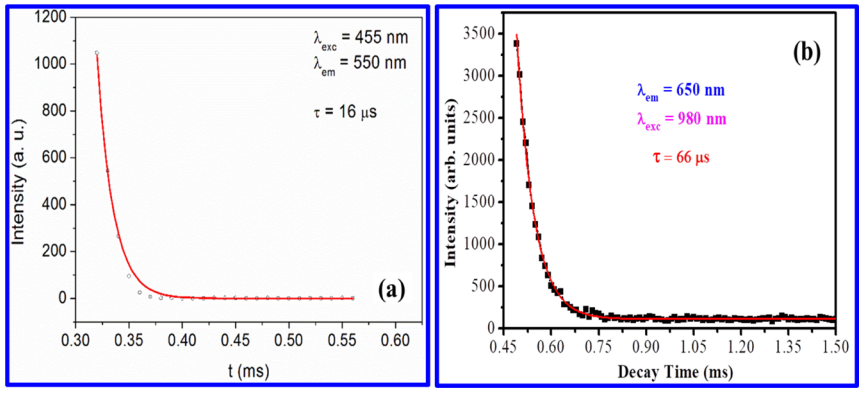

Figure 7. PL decay profiles of the $^5F_5$ level: (a) emission monitored at 550 nm for DC and (b) emission monitored at 650 nm for UC of YVO_4:Ho^{3+}/Yb^{3+}. The excitation wavelengths for DC and UC are fixed at 455 nm and 980 nm, respectively.

https://doi.org/10.1021/acsomega.1c01572
ACS Omega 2021, 6, 19471−19483

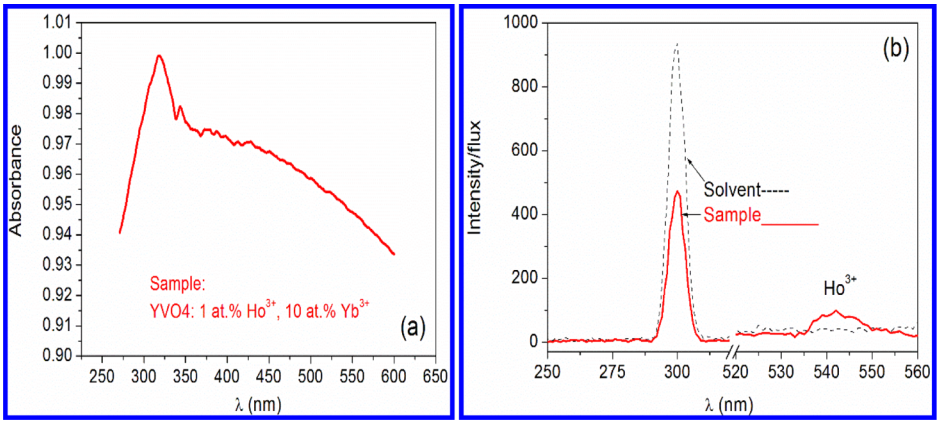

Figure 8. (a) Absorption spectrum of sample YVO_4:1 at. % Ho^{3+}/10 at. % Yb^{3+} and (b) spectra of solvent and the sample for quantum yield analysis.

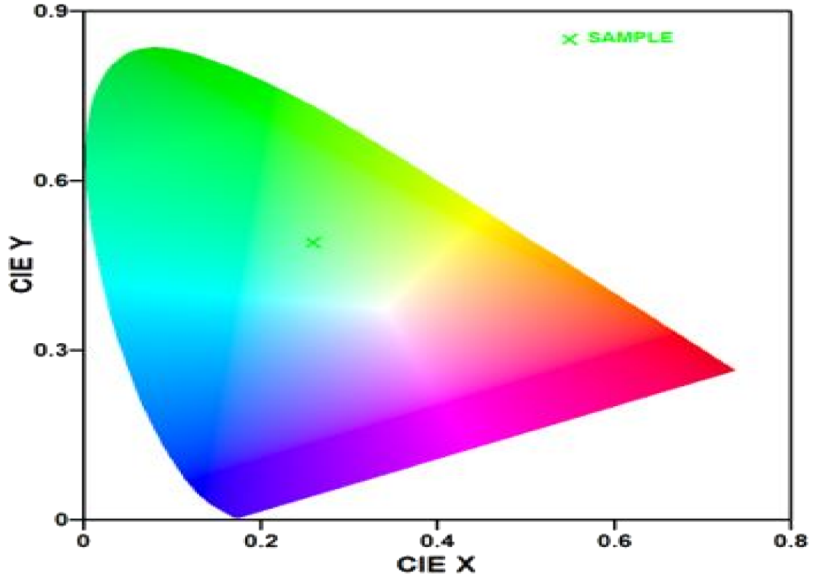

Figure 9. CIE color coordinates of YVO_4:Ho^{3+}/Yb^{3+} upon DC at 300 nm excitation.

The photoluminescence decay of the $^5F_5$ level (650 nm emission) of the Ho^{3+} ion in YVO_4:0.01% Ho^{3+}/0.1% Yb^{3+} under the excitation of 980 nm is shown in Figure 7b. τ is found to be ~66 μs. Similar values of the lifetime were reported for Ho^{3+} ($^5F_5$)-doped nanophosphor in the literature.[16]

2.5.5. Quantum Yield Study. The quantum yield (η) of YVO_4:$x$$Ho^{3+}$, $y$$Yb^{3+}$ (x = 1 at. % and y = 10 at. %) is calculated based on the absolute method using an integrating sphere of diameter 15 cm coated with $BaSO_4$ after standardization (rhodamine B in water: η = 31%). In the present work, we assume that the light falling on $BaSO_4$ particles is perfectly (100%) scattered, and the scattered light is collected by a detector. A sample holder is kept at the center of the integrating sphere, which has two windows: one is for the entrance of the excitation light and another is for the outlet of the scattered light or emitted light, which are captured by the detector.[37] The bandwidths of the excitation and emission wavelengths and iris (%) were fixed during the experiment. It was assumed that solvent did not absorb the excitation light. A very small quantity of the sample was dispersed in solvent. The absorbance value of the sample should be less than 0.1 so that it does not show self-absorption inside the integrating sphere. Upon excitation, the sample containing nanoparticles will absorb and the remaining photons will be scattered from solvent. The number of scattered photons will be less for the sample dispersed in solvent than that from solvent only.

The luminescence quantum yield (η) is defined by the ratio of the number of emitted photons (ε_{phe}) to the absorbed photons (α_{pha}) as follows

$$\eta = \frac{\varepsilon_{phe}}{\alpha_{pha}} = \frac{\int I_{emission}}{I_{solvent} - I_{sample}} \quad (3)$$

where $I_{emission}$ is the luminescence emission spectrum of the sample dispersed in solvent, $I_{solvent}$ is the spectrum of the light used to excite only the solvent (methanol), and I_{sample} is the spectrum of the light used for exciting the sample in solvent. Therefore, the difference between the areas of $I_{solvent}$ and I_{sample} will give us the number of photons absorbed by the sample.

In the present work, 5 mg of the sample (1 at. % Ho^{3+} and 10 at. % Yb^{3+}-doped YVO_4) is dispersed in 10 mL of methanol (solvent). A quartz cuvette is used as the sample holder, and the excitation wavelength was chosen at 300 nm. $I_{solvent}$ and I_{sample} are recorded from 200 to 700 nm. $I_{emission}$ is obtained from I_{sample}. The absorption spectrum of YVO_4:Ho^{3+}/Yb^{3+} is shown in Figure 8a. Typical spectra of the sample and solvent are shown in Figure 8b. A quantum yield of 27% is obtained after excitation at 300 nm. The value of the quantum yield is dependent on the

https://doi.org/10.1021/acsomega.1c01572
ACS Omega 2021, 6, 19471−19483

wavelength of excitation because the number of photons absorbed is dependent on the wavelength of excitation in the case of YVO_4:Ho^{3+}/Yb^{3+} nanophosphor. This is confirmed by various excitations at 300, 325, 425, 455, and 480 nm. The highest quantum yield is obtained at 300 nm. A 5% error may occur during calculation because the emission peak is not sharp.

2.6. Calorimetric Performance Study. The CIE 1931 chromaticity of the YVO_4:xHo^{3+}:yYb^{3+} (x = 1 at. % and y = 10 at. %) nanophosphor upon excitation at 300 nm has been calculated from the luminescence spectra, and the CIE chromaticity coordinates are x = 0.26 and y = 0.49 (Figure 9). The correlated color temperatures (CCT) are calculated using McCamy's third-order polynomial equation[27]

$$\mathrm{CCT} = 449n^3 + 3525n^2 + 6823.3n + 5520.33 \quad (4)$$

where $n = (x - x_e)/(y_e - y)$ is an inverse slope line, in which (x and y) represent the color coordinates of the obtained YVO_4:Ho^{3+}/Yb^{3+} nanophosphor and the epicenter is at x_e = 0.332 and y_e = 0.185. The CCT value is found to be 8620.

It is to be noted that the CIE coordinates upon 980 nm are not provided here because the intensity of the peak around 650 nm is higher than that of the base value obtained at 400 nm by 1.3 times. In another way of expression, the peak intensity around 650 nm is very weak. This means that it loses a high amount of energy upon excitation at 980 nm as well as high background or thermal energy associated with CW laser excitation at 980 nm, which gives higher lattice/phonon energy. While intensity values from 400 to 700 nm wavelengths are added in the CIE chromaticity program, it gives only x = 0.34 and y = 0.33, which is almost white. This is unacceptable because we can see an orange color upon excitation at 980 nm. In view of this, is there a need to change/modify the CIE coordinate program for 980 nm excitation or the UC luminescence study? There are a few reports on the calculation of CIE coordinates using different programs.[38]

2.7. Applications. *2.7.1. Magnetic-Based Hyperthermia Study.* Initially, 1−5 mg of Fe_3O_4@YVO_4:Ho^{3+}/Yb^{3+} hybrid having magnetic−luminescence property (the weight ratio of Fe_3O_4 to YVO_4:Ho^{3+}/Yb^{3+} = 1:4) was dispersed in 1 mL of deionized water in a 1.5 mL microcentrifuge tube and allowed for ultrasonication for 15 min, and this was placed at the center of the induction coil without touching the walls of the coil, and the temperature sensor is dipped in the microcentrifuge tube and here, a radiofrequency of 280 kHz and 310 Oe magnetic field are applied for heat generation. We had evaluated the heating ability of different hybrid magnetic nanoparticles (MNPs) with respect to their concentrations and magnetic fields/currents. The resultant magnetic field generated at the center of the 6 cm copper coil due to the applied current was calculated by using the following formula

$$H = \frac{1.257ni}{l}\ (\mathrm{Oe}) \quad (5)$$

where H is the magnetic field, n is the number of turns in the coil, i is the applied current, and l is the diameter of the turn in cm. The magnetic field produced from the induction coil is directly dependent on the amount of current passing to the coil. For killing cancer cells, the temperature required to attain the hybrid MNP is ∼42 °C.

As shown in Figure 10, the graph of heat generation (T) with time (t) is plotted by taking 1−5 mg/mL hybrid MNPs dispersed in 1 mL of deionized water at a magnetic field of 310 Oe for 10 min, and it is noticed that the hybrids of 1−3 mg/mL

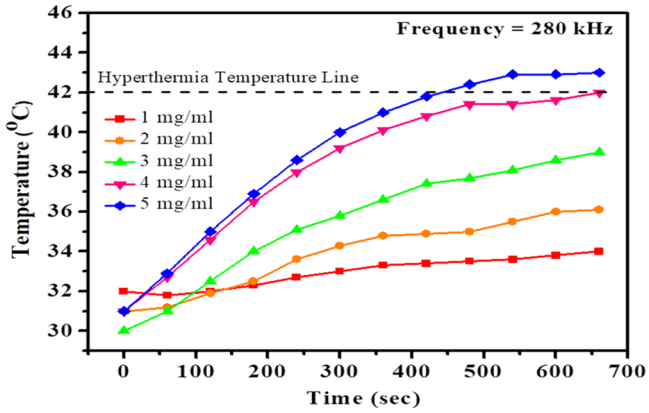

Figure 10. Rise in temperature with time from sample Fe_3O_4@YVO_4:Ho^{3+}/Yb^{3+} hybrid nanoparticles of 1−5 mg/mL.

have not attained the hyperthermia temperature (∼42 °C) and 4 mg/mL of the hybrid nanoparticles has achieved the ∼42 °C temperature at 10 min, but, interestingly, when the 5 mg/mL hybrid is examined, it has attained the hyperthermia temperature in just 7 min.

The specific absorption rate (SAR) is calculated for Fe_3O_4@YVO_4:Ho^{3+}/Yb^{3+} hybrid by using the following equation[39]

$$\mathrm{SAR} = C\left(\frac{\Delta T}{\Delta t}\right)\frac{1}{m_{\mathrm{mag}}} \quad (6)$$

where C is the sample-specific heat capacity, $\Delta T/\Delta t$ is the initial slope of the time-dependent temperature curve, and m_{mag} is the amount of magnetite per total amount of magnetite or Fe and water. The typical SAR value for 5 mg/mL hybrid is calculated to be 138 W/g (g is expressed in terms of weight of Fe_3O_4). These values are higher than those of reported ones in Fe_3O_4 (10−50 W/g) and $LaSrMnO_3$ (20−90 W/g) based MNP systems.[23−25,29,40−44] However, high values of the SAR in $Li_{0.3}Zn_{0.3}Co_{0.1}Fe_{2.3}O_4$ particles (200−350 W/g) were also reported.[45] The high efficacy of SAR values exhibits the utility of hybrid in cancer therapy application.

2.7.2. Hybrid for Potential Imaging. The prepared Fe_3O_4@YVO_4:Ho^{3+}/Yb^{3+} hybrid is highly dispersible in water (Figure 11). This can show magnetic behavior upon bringing a

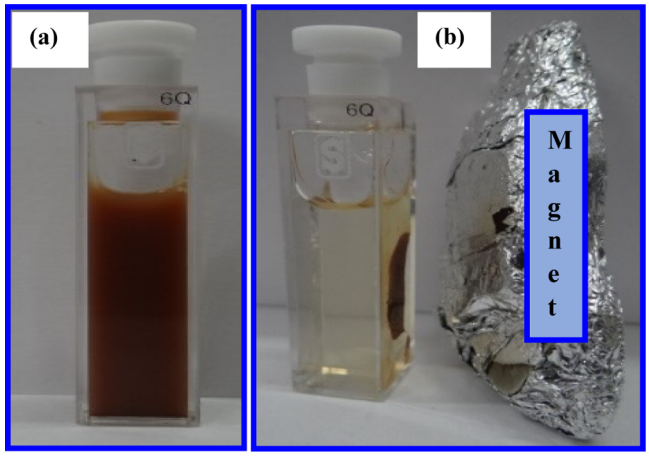

Figure 11. Digital photographs of (a) Fe_3O_4@YVO_4:Ho^{3+}/Yb^{3+} hybrid nanoparticles dispersed in water and (b) same after external magnetic field applied on it.

https://doi.org/10.1021/acsomega.1c01572
ACS Omega 2021, 6, 19471−19483

permanent magnet over a cuvette containing 5 mg of the sample in 3.5 mL of water. Interestingly, this hybrid has chemical bonding among particles due to PEG coating over particles. In the presence of the magnet, it attracts hybrid without leaving YVO_4:Ho^{3+}/Yb^{3+}, which is nonmagnetic. This can be visualized by the appearance of transparency in water after bringing the magnet over the cuvette. Pure Fe_3O_4 dispersed in water appears black in color. Pure YVO_4:Ho^{3+}/Yb^{3+} appears white in color. In the case of hybrid, it appears brownish in color.

Upon UV excitation at 300 nm, the magnetic−luminescent hybrid nanophosphor shows the V−O band at 400−500 nm, and also, Ho^{3+} peaks are observed at 550, 650, and ∼755 nm (Figure 12). However, we have calculated the integrated peak

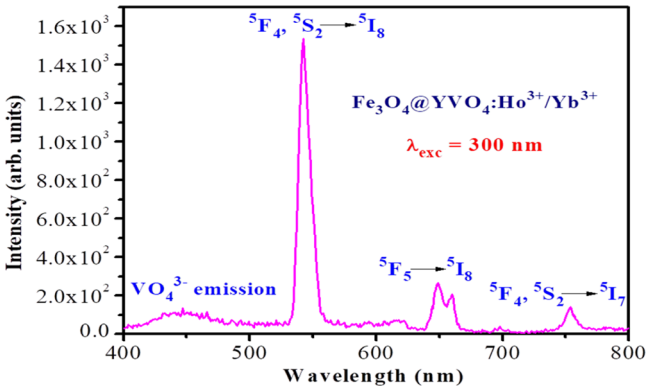

Figure 12. DC emission spectrum of Fe_3O_4@YVO_4:Ho^{3+}/Yb^{3+} hybrid monitored at λ_{exc} = 300 nm showing the V−O CTB at 400−500 nm and Ho^{3+} peaks at 550, 650, and 755 nm.

area, and it is observed that hybrid has two times less intensity as compared to that of pure YVO_4:Ho^{3+}/Yb^{3+} nanophosphor. This is due to the association of magnetic Fe_3O_4 nanoparticles in hybrid.

2.7.3. YVO_4:Ho^{3+}/Yb^{3+} for Anticounterfeiting Applications. Furthermore, the prepared nanophosphor material exhibits its potentiality for anticounterfeiting applications. There are reports on the use of nanoparticles for anticounterfeiting applications.[46] Most of the reported anticounterfeiting applications are based on UV light excitation.[46,47] However, reports on NIR light excitation based anticounterfeiting applications are very less due to small-sized spots of the laser (1−2 mm in diameter) that it cannot cover larger areas (a few cm in any dimensions), which can be done easily by UV light.[48,49] In this work, we overcome this problem using a proper collimator as well as a suitable filter. For its implication, a demonstration has been carried out by dispersing the YVO_4:Ho^{3+}/Yb^{3+} nanophosphor into methanol and dispersed particles are used to write letters or numerals over a sheet of paper (shown in Figure 13). We are able to write A, B, C, D... letters as well as 1, 2, 3... numerals and are able to see them under 980 nm excitation. Therefore, it is evident that the prepared nanomaterial will be a potential asset for anticounterfeiting applications.

2.7.4. Sorption Studies of Au^{3+} Ions on YVO_4:Ho^{3+}/Yb^{3+} Nanophosphor by Using the Instrumental NAA Technique. 10, 50, and 100 ppm of Au^{3+} solutions are prepared. 50 mg of the sample YVO_4:1 at. % Ho^{3+}/10 at. % Yb^{3+} is added to every Au^{3+} solution. It is kept for 24 h. The supernatant liquid is separated from the sample by centrifugation. The adsorption studies of the supernatant liquid are carried out at the Dhruva research reactor,

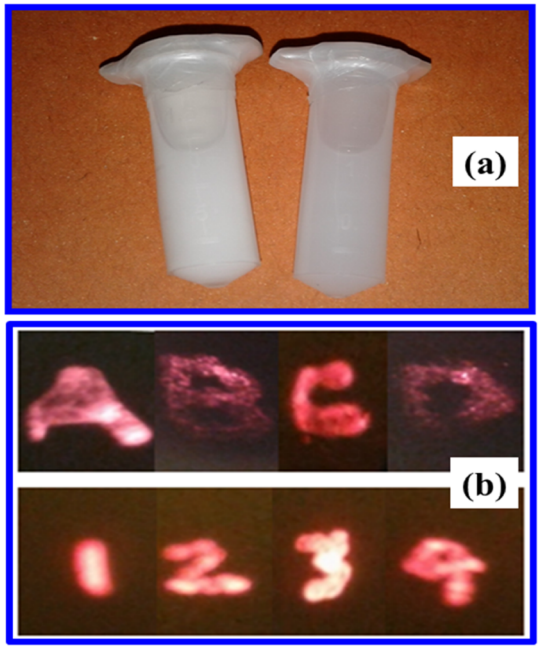

Figure 13. Security ink: (a) YVO_4:Ho^{3+}/Yb^{3+} nanophosphors are dispersed into methanol and dispersed particles are used to write letters or numerals over a sheet of paper. (b) Photographs of A, B, C, D... letters as well as 1, 2, 3... numerals written. Without 980 nm NIR light excitation, these could not be seen. Under 980 nm excitation, these are seen. As we use the bandwidth filter (450−700 nm) before the camera, we are able to see the actual color because other lights (λ < 400 nm or >700 NIR-IR range) are eliminated by the use of the bandwidth filter. Also, to see larger spots, proper collimators are used.

BARC, Mumbai.[50] The control (10, 50, and 100 ppm solution of Au^{3+} ions) and supernatant liquid are examined by instrumental NAA using short irradiations at the pneumatic carrier facility of the Dhruva research reactor (for 1 min at 5×10^{13} n/cm^2/s flux), and the uptake of Au^{3+} ions is analyzed using its activation product ^{198}Au (multi-γ ray-like 411 keV). The decay of γ rays from Au^{3+} is counted by using a high purity germanium detector. Figure 14 shows that the amounts of absorption of Au^{3+} at 10, 50, and 100 ppm are 17, 21, and 25%, respectively, per 50 mg of the sample and 0.34, 0.42, and 0.50%, respectively, per 1 mg of

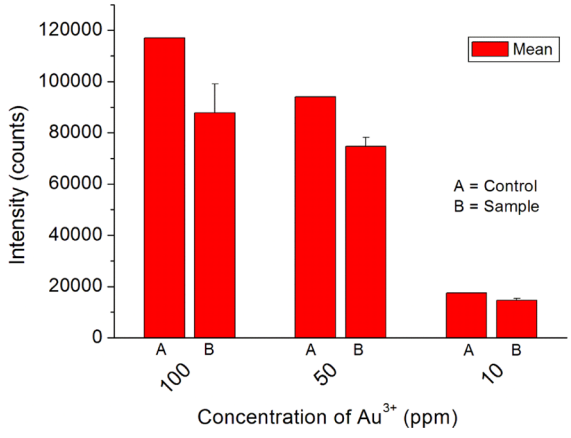

Figure 14. Counts obtained from the NAA experiment. A means control (100, 50, and 10 ppm of Au^{3+}). Solution was prepared in water medium. B means the supernatant liquid after absorption of Au^{3+} ions by 50 mg of sample YVO_4:Ho^{3+}/Yb^{3+}.

https://doi.org/10.1021/acsomega.1c01572
ACS Omega 2021, 6, 19471−19483

the sample. There were reports on the use of hybrid nanoparticles with Au for improvement in X-ray contrast agents due to their nontoxicity and very high absorption cross section.[51]

2.7.5. Zeta Potential Study. To extract the information about the net surface charge associated with nanoparticles, the zeta potential experiment is carried out. These values can be used to determine the particle tendency to aggregate in aqueous solution and to provide the physicochemical properties of nanoparticles required for *in vitro* and *in vivo* research experiments. The zeta potential (ζ) of the particles dispersed in deionized water is recorded. The ζ values of YVO_4:Ho^{3+}/Yb^{3+} are found to be +0.3, −5.0, and −7.0 mV at pH = 5, 7, and 8, respectively. These values are suitable for bioimaging applications.

3. EXPERIMENTAL SECTION

3.1. Materials and Methods. The chemicals used were yttrium(III) acetate [$(CH_3CO_2)_3Y{\cdot}xH_2O$, 99.99%, Sigma-Aldrich], holmium(III) acetate [$(CH_3CO_2)_3Ho{\cdot}xH_2O$, 99.99%, Sigma-Aldrich], ytterbium(III) acetate [$(CH_3CO_2)_3Yb{\cdot}xH_2O$, 99.99%, Sigma-Aldrich], ammonium metavanadate (NH_4VO_3, 99.99%, Sigma-Aldrich), EG ($HOCH_2CH_2OH$), PEG (6000), sodium hydroxide (NaOH), and dilute HCl acid for the synthesis of $Y_{0.89}Ho_{0.01}Yb_{0.10}VO_4$ (YVO_4:Ho^{3+}/Yb^{3+}) nanoparticles.

3.2. Synthesis of YVO_4:Ho^{3+}/Yb^{3+} Nanoparticles. Figure S6 represents the synthesis procedure of 1 at. % of Ho^{3+} and 10 at. % of Yb^{3+} doped YVO_4 luminescent nanoparticles (YVO_4:Ho^{3+}, Yb^{3+}) prepared by the polyol-mediated synthesis. In the typical synthesis, 603.7 mg of $(CH_3CO_2)_3Y{\cdot}xH_2O$, 8.7 mg of $(CH_3CO_2)_3Ho{\cdot}xH_2O$, and 89.24 mg of $(CH_3CO_2)_3Yb{\cdot}xH_2O$ were taken and dissolved in 5 mL of concentrated HCl acid and heated until they got dissolved. A clear and transparent solution of metal ions was obtained. In order to remove excess HCl, the solution was further evaporated by alternate additions of 10 mL of deionized water, followed by heating (∼80 °C). The evaporation process was repeated at least five times. Moreover, 298.2 mg of NH_4VO_3 was dissolved in 10 mL of deionized water. In order to make a clear solution, 2.64 g of NaOH was dissolved in 10 mL of deionized water. It was added dropwise to NH_4VO_3 solution, and it finally became transparent. The evaporated solution of metal ions was transferred into a 100 mL round bottom flask, and 20 mL of EG was added and refluxed for 10 min at 70 °C and then NH_4VO_3 solution was added dropwise. A pale yellow color was observed while adding NH_4VO_3 solution in the round bottom flask; finally, the color changed from pale yellow to white after heating at 120 °C for 2 h. A white precipitate was obtained and allowed to cool at room temperature. It was centrifuged at 5000 rpm for 5 min and washed with 10 mL of acetone twice and dried under an IR lamp to collect the dry powder. The prepared sample was heated at 900 °C for 4 h.

Similarly, various Ho^{3+} concentrations (3, 5, and 7 at. %) and fixed amounts of Yb^{3+} (10 at. %) doped YVO_4 nanoparticles have been prepared. The as-prepared samples were further annealed at 900 °C for 4 h.

3.3. Synthesis of Magnetic−Luminescent Hybrid Nanoparticles for Hyperthermia. *3.3.1. Preparation of PEG-Coated Fe_3O_4 MNPs.* The preparation of Fe_3O_4 nanoparticles by the coprecipitation method was carried out using the following steps:

Step (A): 1.0 g of $FeSO_4{\cdot}7H_2O$ and 0.972 g of $FeCl_3{\cdot}6H_2O$ in 1:2 molar ratios were taken. $FeSO_4.7H_2O$ was dissolved dropwise in 50 mL of deionized water under continuous stirring in a beaker with a glass rod until there appears clear pale yellow color solution. A solution of $FeCl_3{\cdot}6H_2O$ was prepared in another beaker. Under continuous stirring of ferrous sulfate, the solution of ferric chloride was added to it. To this solution, 30 mL of 12 M NH_4OH solution was added dropwise under constant stirring. A black color precipitate was formed and kept for 1 h. To collect the Fe_3O_4 MNPs, a strong magnet of 2.5 kOe was placed at the bottom of the beaker for 24 h so that they settle down, and the supernatant liquid was removed by using a micropipette. The collected Fe_3O_4 nanoparticles were washed with deionized water to remove excess NH_3, and also, finally, it was washed twice with acetone to remove excess water present in Fe_3O_4 nanoparticles. This is shown in the schematic diagram in Figure S7. Here, the reaction can be represented as follows

$$Fe^{2+} + 2Fe^{3+} + 8OH^- \rightarrow Fe_3O_4 + 4H_2O$$

Step (B): 25 mg of Fe_3O_4 MNPs (Fe_3O_4-MNPs) prepared in step (A) were transferred into another beaker which contained 1 g of PEG which was already dissolved in 10 mL of deionized water. It was allowed for ultrasonication for 1 h. In this way, the surface of the Fe_3O_4-MNPs was coated with PEG, and the prepared sample was highly dispersible in water. Furthermore, the as-prepared sample was centrifuged, washed with 10 mL of acetone twice, and dried under an IR lamp for collecting the dry sample.

4.3.2. Preparation of PEG-Coated YVO_4 Luminescent Nanoparticles. Step (C): 100 mg of the 900 °C heated sample of YVO_4: 1 at. % Ho, 10 at. % Yb was added to a beaker containing 5 g of PEG in 10 mL of deionized water. It was ultrasonicated for 1 h and then centrifuged and washed with 10 mL of acetone twice. It was dried under an IR lamp. The schematic diagram is shown in Figure S8.

4.4. Preparation of Fe_3O_4@YVO_4:Ho^{3+}/Yb^{3+} Hybrid Magnetic−Luminescent Nanoparticles. The abovementioned powder samples from PEG-coated Fe_3O_4 (step B) and YVO_4: 1 at. % Ho, 10 at. % Yb (step C) were mixed in a weight ratio of 1:4 in a beaker. 5 g of PEG dissolved in 10 mL of deionized water was added to the beaker and ultrasonicated for 1 h. The powder was collected after centrifugation, washed with acetone, and kept under an IR lamp for 1 h. This powder is considered as Fe_3O_4@YVO_4:Ho^{3+}/Yb^{3+} hybrid. The schematic diagram for the formation of the hybrid is shown in Figure S9.

4.5. Characterization Techniques. The XRD patterns of as-prepared and 900 °C heated samples were recorded using a PAN analytical powder X-ray diffractometer with a Ni filter having Cu K_α (1.5405 Å) radiation at 40 kV and 30 mA. The interplanar distance (d_{hkl}) of the plane (hkl) in a lattice was calculated using the Bragg's relation: $2d_{hkl} \sin\theta = n\lambda$, where, λ represents the X-ray wavelength of Cu K_α and θ represents the Bragg's angle. The average crystallite size (D) was estimated by using the Debye−Scherrer relation: $D = 0.9\lambda/(\beta \cos\theta)$, where β represents the full width at half maximum of the hkl plane.

Thermal analysis of the as-prepared sample (YVO_4: 1 at. % Ho, 10 at. % Yb) was carried out using TG−DTA and EGA Setaram (Setsys evolution) in an argon atmosphere in the range 30−900 °C.

The vibrational structure of the synthesized samples was studied by using FTIR spectroscopy (Bomem MB 102 spectrophotometer) with a 1 cm^{-1} resolution.

The surface morphology of Ho^{3+}- and Yb^{3+}-doped YVO_4 particles was investigated using a scanning electron microscope , and EDX analysis was carried out using a field emission scanning

https://doi.org/10.1021/acsomega.1c01572
ACS Omega 2021, 6, 19471−19483

electron microscope coupled with EDX (Quanta FEG 450, FEI, Netherland). The particle morphology was examined using a transmission electron microscope instrument (2000 FX, JEOL, Japan).

The excitation and emission spectra of all the samples were recorded using EDINBURGH Instrument FLS920 equipped with a 450 W xenon arc lamp having Peltier element cooled red sensitive Hamamatsu R955 PMT and a microsecond lamp (100 W) for the luminescence decay study.

For the UC study, a 980 nm laser diode (maximum power = 5 W) of CW has been used, and the luminescence decay was recorded using the pulse mode facility available in this setup. The detector was the same as in EDINBURGH Instrument FLS920.

The heating experiment of the hybrid nanoparticles under an AC magnetic field was performed in a 1.5 mL microcentrifuge tube, which was placed at the center of a copper coil having a diameter of 6 cm (Faraday Power System unit, Bangalore, India).

4. CONCLUSIONS

In summary, YVO_4:0.01Ho^{3+}/0.1Yb^{3+} nanophosphor is synthesized by a polyol-mediated synthesis route. The as-prepared sample is further annealed to 900 °C to improve its crystallinity and to remove organic moieties and the water molecules present in the sample. The XRD study has confirmed the tetragonal phase with space group $I4_1/amd$. YVO_4:0.01Ho^{3+}/0.1Yb^{3+} exhibits strong upconverted green and red color bands at ∼550 nm ($^5F_4$, $^5S_2 \rightarrow {}^5I_8$), ∼650 nm ($^5F_5 \rightarrow {}^5I_8$), and ∼755 nm ($^5F_4$, $^5S_2 \rightarrow {}^5I_7$) of Ho^{3+} under 980 nm excitation. At 300 nm excitation, a broad emission peak at 400−500 nm along with Ho^{3+} characteristic peaks are observed. The broad emission band is arising mainly due to ligand to metal CT (V−O CTB). The green and red bands are observed due to two-photon absorption, which is confirmed by the power-dependent UC study. The critical distance (*Rc*) values for excitations at 300 and 455 nm are found to be 4.2 and 24.6 Å, respectively. The critical distance (R_c) between VO_4^{3-} and Ho^{3+} ions depend on both the exchange interaction and multipole−multipole interaction. The synthesized nanophosphor material exhibits its potentiality in gold detection/adsorption. Furthermore, the hybrid nanomaterial reveals its bifunctional behavior (luminescence as well as magnetic−luminescence). This hybrid material has attained the hyperthermia temperature of ∼42 °C under the applied AC magnetic field. The synthesized nanophosphor is manifesting its promising potentiality in luminescence properties, anticounterfeiting and hyperthermia applications.

■ ASSOCIATED CONTENT

Supporting Information

The Supporting Information is available free of charge at https://pubs.acs.org/doi/10.1021/acsomega.1c01572.

XRD patterns of 900 °C annealed YVO_4:Ho^{3+}/Yb^{3+}, Fe_3O_4, Fe_3O_4@PEG, and Fe_3O_4@YVO_4:Ho^{3+}/Yb^{3+} along with JCPDS no. 76-1649 of pure YVO_4, TGA and DTA curves of as-prepared YVO_4:Ho^{3+}/Yb^{3+}, FT-IR spectra of YVO_4:Ho^{3+}/Yb^{3+}, Fe_3O_4, PEG, Fe_3O_4@PEG, and Fe_3O_4@ YVO_4:Ho^{3+}/Yb^{3+}, vibrational bands involved in the 900 °C annealed YVO_4:Ho^{3+}/Yb^{3+}, PEG, Fe_3O_4@PEG, and Fe_3O_4@YVO_4:Ho^{3+}/Yb^{3+}, SEM micrograph of 900 °C annealed sample of $Y_{1-xy}VO_4$:Ho_x^{3+}/Yb_y^{3+} nanophosphor, elemental mapping, and EDX spectrum, chemical composition of the surface of YVO_4:Ho^{3+}/Yb^{3+} nanophosphor from EDX analysis, TEM image of 900 °C annealed YVO_4:Ho^{3+}/Yb^{3+} nanophosphor, schematic diagram for the preparation of YVO_4:Ho^{3+}/Yb^{3+} nanophosphor, schematic diagram for the preparation of PEG-coated Fe_3O_4-MN, schematic diagram for the preparation of PEG-coated YVO_4:1 at. % Ho^{3+}/10 at. % Yb^{3+}, and schematic representation for the preparation and formation of the magnetic−luminescent hybrid nanoparticles Fe_3O_4@YVO_4:Ho^{3+}/Yb^{3+} (PDF)

■ AUTHOR INFORMATION

Corresponding Authors

Bheeshma Pratap Singh − *Chemistry Division, Bhabha Atomic Research Centre, Mumbai 400085, India;* orcid.org/0000-0001-9109-1515; Phone: +91-22-25592321; Email: bheeshmapratap@gmail.com

Venkata Nagendra Kumar Putta − *Department of Chemistry, GITAM University, Hyderabad 502329, India*; Phone: +91-9885357559; Email: pvenkatanagendrakumar@gmail.com

Raghunath Acharya − *Radiochemistry Division, Bhabha Atomic Research Centre, Mumbai 400085, India; Homi Bhabha National Institute, Mumbai 400094, India*; Phone: +91-22-25594590; Email: racharya@barc.gov.in

Raghumani Singh Ningthoujam − *Chemistry Division, Bhabha Atomic Research Centre, Mumbai 400085, India; Homi Bhabha National Institute, Mumbai 400094, India;* orcid.org/0000-0002-4642-5990; Phone: +91-22-25592321; Email: rsn@barc.gov.in

Authors

Ramaswamy Sandeep Perala − *Department of Chemistry, GITAM University, Hyderabad 502329, India; Chemistry Division and Radiochemistry Division, Bhabha Atomic Research Centre, Mumbai 400085, India*

Rashmi Joshi − *Chemistry Division, Bhabha Atomic Research Centre, Mumbai 400085, India; Homi Bhabha National Institute, Mumbai 400094, India;* orcid.org/0000-0002-6816-8833

Complete contact information is available at: https://pubs.acs.org/10.1021/acsomega.1c01572

Notes

The authors declare no competing financial interest.

■ ACKNOWLEDGMENTS

This work is a part of the Ph.D. thesis of R.S.P. This work was carried out as a part of the UGC-DAE-CRS project (CRS-M-285) on "Studies on lanthanides, actinides (U and Th), and toxic elements using nanoparticle-based solid adsorbents and NAA". B.P.S. acknowledges the award through Inspire Faculty (IFA17-MS-109) provided by DST, Government of India. The authors thank Dr. A. K. Tyagi, Chemistry Group, BARC, Dr. P. A. Hassan, Chemistry Division, BARC, and Dr. P. K. Pujari, Radiochemistry Group, BARC, for their support and encouragement during this work.

■ REFERENCES

(1) Downing, E.; Hesselink, L.; Ralston, J.; Macfarlane, R. Three-Colour, Solid-State, Three-Dimensional Display. *Science* **1996**, *273*, 1185−1189.

(2) Chatterjee, D. K.; Zhang, Y. Upconverting Nanoparticles as Nano-Transducers for Photodynamic Therapy in Cancer Cells. *Nanomedicine* **2008**, *2*, 69−72.
(3) Liu, Q.; Feng, W.; Yang, T.; Yi, T.; Li, F. Upconversion Luminescence Imaging of Cells and Small Animals. *Nat. Protoc.* **2013**, *8*, 2033−2044.
(4) Chen, J.; Zhao, J. X. Upconversion Nanomaterials: Synthesis, Mechanism, and Applications in Sensing. *Sensors* **2012**, *12*, 2414−2435.
(5) Prasad, A. I.; Singh, L. R.; Joshi, R.; Ningthoujam, R. S. Luminescence study on crystalline phase of $Y_2Si_2O_7$ from mesoporous silica and Y_2O_3: Ln^{3+} at 900 °C. *AIP Adv.* **2018**, *8*, 105310.
(6) Mir, W. J.; Sheikh, T.; Arfin, H.; Xia, Z.; Nag, A. Lanthanide doping in metal halide perovskite nanocrystals: spectral shifting, quantum cutting and optoelectronic applications. *NPG Asia Mater.* **2020**, *12*, 9.
(7) Sehrawat, P.; Dayawati; Boora, P.; Malik, R. K.; Khatkar, S. P.; Taxak, V. B. Achieving orange red emission with high color purity from novel perovskite based $Sr_9Al_6O_{18}$:Sm^{3+} nano-cubes for advanced optoelectronic applications. *Ceram. Int.* **2021**, *47*, 5432−5445.
(8) Ningthoujam, R. S.; Singh, L. R.; Sudarsan, V.; Dorendrajit Singh, S. Energy Transfer Process and Optimum Emission Studies in Luminescence of Core-Shell Nanoparticles: YVO_4:Eu−YVO_4 and surface state analysis. *J. Alloys Compd.* **2009**, *484*, 782−789.
(9) Ningthoujam, R. S.; Shukla, R.; Vatsa, R. K.; Duppel, V.; Kienle, L.; Tyagi, A. K. Gd_2O_3:Eu^{3+} Particles Prepared by Glycine-Nitrate Combustion: Phase, Concentration, Annealing, and Luminescence Studies. *J. Appl. Phys.* **2009**, *105*, 084304.
(10) Yaiphaba, N.; Ningthoujam, R. S.; Singh, N. R.; Vatsa, R. K. Luminescence Properties of Redispersible Tb^{3+}-Doped $GdPO_4$ Nanoparticles Prepared by an Ethylene Glycol Route. *Eur. J. Inorg. Chem.* **2010**, 2682−2687.
(11) Shanta Singh, N.; Ningthoujam, R. S.; Dorendrajit Singh, S.; Viswanadh, B.; Manoj, N.; Vatsa, R. K. Preparation of Highly Crystalline Blue Emitting MVO_4:Tm^{3+} (M=Gd, Y) Spherical Nanoparticles: Effects of Activator Concentration and Annealing Temperature on Luminescence, Lifetime and Quantum yield. *J. Lumin.* **2010**, *130*, 2452−2459.
(12) Shanta Singh, N.; Ningthoujam, R. S.; Phaomei, G.; Singh, S. D.; Vinu, A.; Vatsa, R. K. Re-Dispersion and Film Formation of $GdVO_4$:Ln^{3+} (Ln^{3+} = Dy^{3+}, Eu^{3+}, Sm^{3+}, Tm^{3+}) Nanoparticles: Particle Size and Luminescence Studies. *Dalton Trans.* **2012**, *41*, 4404−4412.
(13) Parchur, A. K.; Ningthoujam, R. S. Preparation and Structure Refinement of Eu^{3+} Doped $CaMoO_4$ Nanoparticles. *Dalton Trans.* **2011**, *40*, 7590−7594.
(14) Ningthoujam, R. S. *Enhancement of Photoluminescence by Rare Earth Ions Doping in Semiconductor Inorganic*; Rai, S. B., Dwivedi, Y., Eds.; Nova Science Publishers Inc.: USA, 2012; Chapter 6, pp 145−182.
(15) Dwivedi, A.; Rai, E.; Kumar, D.; Rai, S. B. Effect of Synthesis Techniques on the Optical Properties of Ho^{3+}/Yb^{3+} Co-doped YVO_4 Phosphor: A Comparative Study. *ACS Omega* **2019**, *4*, 6903−6913.
(16) Kumar Mahata, M.; Koppe, T.; Kumar, K.; Hofsäss, H.; Vetter, U. Demonstration of Temperature Dependent Energy Migration in Dual-Mode YVO_4:Ho^{3+}/Yb^{3+} Nanocrystals for Low Temperature Thermometry. *Sci. Rep.* **2016**, *6*, 36342.
(17) Soni, A. K.; Joshi, R.; Singh, B. P.; Kumar, N. N.; Ningthoujam, R. S. Near Infrared- and Magnetic-Field-Responsive $NaYF_4$:Er^{3+}/Yb^{3+}@SiO_2@AuNP@Fe_3O_4 Nanocomposites for Hyperthermia Applications Induced by Fluorescence Resonance Energy Transfer and Surface Plasmon Absorption. *ACS Appl. Nano Mater.* **2019**, *2*, 7350−7361.
(18) Soni, A. K.; Yadav, K. K.; Singh, B. P.; Joshi, R.; Chakraborty, S.; Chakravarty, R.; Nagaraja, N. K.; Singh, D. K.; Kain, V.; Dash, A.; Ningthoujam, R. S. Smart YPO_4:Er-Yb Nanophosphor for Optical Heating, Hyperthermia, Security Ink, Cancer Endoradiotherapy and Uranyl Recovery. *ACS Appl. Nano Mater.* **2020**, *4*, 850−860.
(19) Singh, B. P.; Parchur, A. K.; Singh, R. K.; Ansari, A. A.; Singh, P.; Rai, S. B. Structural and Up-Conversion Properties of Er^{3+} and Yb^{3+} Co-doped $Y_2Ti_2O_7$ phosphors. *Phys. Chem. Chem. Phys.* **2013**, *15*, 3480−3489.
(20) Laurent, S.; Forge, D.; Port, M.; Roch, A.; Robic, C.; Vander Elst, L.; Muller, R. N. Magnetic Iron Oxide Nanoparticles: Synthesis, Stabilization, Vectorization, Physicochemical Characterizations, and Biological Applications. *Chem. Rev.* **2008**, *108*, 2064−2110.
(21) Chakraborty, S.; Sharma, K. S.; Rajeswari, A.; Vimalnath, K. V.; Sarma, H. D.; Pandey, U.; Jagannath, J.; Ningthoujam, R. K.; Dash, A. Radiolanthanide-Loaded Agglomerated Fe_3O_4 Nanoparticles for Possible use in the Treatment of Arthritis: Formulation, Characterization and Evaluation in Rats. *J. Mater. Chem. B* **2015**, *3*, 5455−5466.
(22) Das, T. Applications of Radioisotopes in Medicine. *Sci. Cult.* **2015**, *81*, 230−236.
(23) Parchur, A. K.; Ansari, A. A.; Singh, B. P.; Hasan, T. N.; Syed, N. A.; Rai, S. B.; Ningthoujam, R. S. Enhanced luminescence of $CaMoO_4$:Eu by Core@Shell Formation and its Hyperthermia Study after Hybrid Formation with Fe_3O_4:Cytotoxicity Assessment on Human Liver Cancer Cells and Mesenchymal Stem Cells. *Integr. Biol.* **2014**, *6*, 53−64.
(24) Prasad, A. I.; Parchur, A. K.; Juluri, R. R.; Jadhav, N.; Pandey, B. N.; Ningthoujam, R. S.; Vatsa, R. K. Bi-Functional Properties of Fe_3O_4@YPO_4:Eu Hybrid Nanoparticles: Hyperthermia Application. *Dalton Trans.* **2013**, *42*, 4885−4896.
(25) Jain, N.; Singh, R. K.; Singh, B. P.; Srivastava, A.; Singh, R. A.; Singh, J. Enhanced Temperature-Sensing Behavior of Ho^{3+}-Yb^{3+}-Codoped $CaTiO_3$ and Its Hybrid Formation with Fe_3O_4 Nanoparticles for Hyperthermia. *ACS Omega* **2019**, *4*, 7482−7491.
(26) Huang, C.-C.; Chuang, K.-Y.; Chou, C.-P.; Wu, M.-T.; Sheu, H.-S.; Shieh, D.-B.; Tsai, C.-Y.; Su, C.-H.; Lei, H.-Y.; Yeh, C.-S. Size-Control Synthesis of Structure Deficient Truncated Octahedral $Fe_{3-\delta}O_4$ Nanoparticles: High Magnetization Magnetites as Effective Hepatic Contrast Agents. *J. Mater. Chem.* **2011**, *21*, 7472.
(27) Hernández-Andrés, J.; Lee, R. L., Jr.; Romero, J. Calculating Correlated Colour Temperatures across the Entire Gamut of Daylight and Skylight Chromaticities. *Appl. Opt.* **1999**, *38*, 5703−5709.
(28) Shannon, R. D. Revised Effective Ionic Radii and Systematic Studies of Interatomic Distances in Halides and Chalcogenides. *Acta Crystallogr.* **1976**, *32*, 751−767.
(29) Sharma, K. S.; Ningthoujam, R. S.; Dubey, A. K.; Chattopadhyay, A.; Phapale, S.; Juluri, R. R.; Mukherjee, S.; Tewari, R.; Shetake, N. G.; Pandey, B. N.; Vatsa, R. K. Synthesis and Characterization of Monodispersed Water Dispersible Fe_3O_4 Nanoparticles and *in vitro* Studies on Human Breast Carcinoma Cell Line under Hyperthermia Condition. *Sci. Rep.* **2018**, *8*, 14766.
(30) Auzel, F. Upconversion and Anti-Stokes Processes with f and d Ions in Solids. *Chem. Rev.* **2004**, *104*, 139−174.
(31) Payne, S. A.; Chase, L. L.; Smith, L. K.; Kway, W. L.; Krupke, W. F. Infrared Cross - Section Measurements for Crystals Doped with Er^{3+}, Tm^{3+}, and Ho^{3+}. *IEEE J. Quant. Electron.* **1992**, *28*, 2619−2630.
(32) Blasse, G. Energy Transfer in Oxidic Phosphors. *Phys. Lett. A* **1968**, *28*, 444−445.
(33) Li, K.; Deun, R. V. Low-Temperature Solid-State Synthesis and Upconversion Luminescence Properties in (Na/Li)Bi$(MoO_4)_2$:Yb^{3+},Er^{3+} and Color Tuning in (Na/Li)Bi$(MoO_4)_2$:Yb^{3+},Ho^{3+},Ce^{3+} Phosphors. *Inorg. Chem.* **2019**, *58*, 6821−6831.
(34) Li, K.; Van Deun, R. Mutual energy transfer luminescent properties in novel $CsGd(MoO_4)_2$:Yb^{3+},Er^{3+}/Ho^{3+} phosphors for solid-state lighting and solar cells. *Phys. Chem. Chem. Phys.* **2019**, *21*, 4746−4754.
(35) Perala, R. S.; Singh, B. P.; Putta, V. N. K.; Acharya, R.; Ningthoujam, R. S. Enrichment of Crystal Field Modification via Incorporation of Alkali K^+ Ions in YVO_4:Ho^{3+}/Yb^{3+} Nanophosphor and Its Hybrid with Superparamagnetic Iron Oxide Nanoparticles for Optical, Advanced Anticounterfeiting, Uranyl Detection, and Hyperthermia Applications. *ACS Omega*. DOI: 10.1021/acsomega.1c01813.
(36) Lisiecki, R.; Dominiak-Dzik, G.; Ryba-Romanowski, W.; Łukasiewicz, T. Conversion of Infrared Radiation into Visible Emission in YVO_4 Crystals doped with Ytterbium and Holmium. *J. Appl. Phys.* **2004**, *96*, 6323−6330.

(37) Singh, B. P.; Parchur, A. K.; Ningthoujam, R. S.; Ansari, A. A.; Singh, P.; Rai, S. B. Enhanced Photoluminescence in $CaMoO_4$:Eu^{3+} by Gd^{3+} Co-doping. *Dalton Trans.* **2014**, *43*, 4779−4789.
(38) Wyszecki, G. Colour Appearance. In *Handbook of Perception and Human Performance, Vol I: Sensory Processes and Perception*; Boff, K. R., Kaufman, L., Thomas, J. P., Eds.; John Wiley & Sons: New York; Chapter 8, 1986.
(39) Joshi, R.; Perala, R. S.; Srivastava, M.; Singh, B. P.; Ningthoujam, R. S. Heat Generation from Magnetic Fluids under Alternating Current Magnetic Field or Induction Coil for Hyperthermia-Based Cancer Therapy: Basic Principle. *J. Rad. Can. Res.* **2019**, *10*, 156−164.
(40) Thorat, N. D.; Patil, R. M.; Khot, V. M.; Salunkhe, A. B.; Prasad, A. I.; Barick, K. C.; Ningthoujam, R. S.; Pawar, S. H. Highly Water Dispersible Surface Functionalized LSMO Nanoparticles for Magnetic Fluid Hyperthermia Application. *New J. Chem.* **2013**, *37*, 2733.
(41) Shete, P. B.; Patil, R. M.; Ningthoujam, R. S.; Ghosh, S. J.; Pawar, S. H. Magnetic Core Shell Structures for Magnetic Fluid Hyperthermia Therapy Application. *New J. Chem.* **2013**, *37*, 3784−3792.
(42) Majeed, J.; Pradhan, L.; Ningthoujam, R. S.; Vatsa, R. K.; Bahadur, D.; Tyagi, A. K. Enhanced Specific Absorption Rate in Silanol Functionalized Fe_3O_4 core - shell Nanoparticles: Study of Fe Leaching in Fe_3O_4 and Hyperthermia in L929 and HeLa cells. *Colloids Surf., B* **2014**, *122*, 396−403.
(43) Thorat, N. D.; Khot, V. M.; Salunkhe, A. B.; Ningthoujam, R. S.; Pawar, S. H. Functionalization of $La_{0.7}Sr_{0.3}MnO_3$ Nanoparticles with Polymer: Studies on Enhanced Hyperthermia and Biocompatibility Properties for Biomedical Applications. *Colloids Surf., B* **2013**, *104*, 40−47.
(44) Thorat, N. D.; Otari, S. V.; Patil, R. M.; Bohara, R. A.; Yadav, H. M.; Koli, V. B.; Chaurasia, A. K.; Ningthoujam, R. S. Synthesis, characterization and biocompatibility of chitosan functionalized superparamagnetic nanoparticles for heat activated curing of cancer cells. *Dalton Trans.* **2014**, *43*, 17343−17351.
(45) Dalal, M.; Greneche, J.-M.; Satpati, B.; Ghzaiel, T. B.; Mazaleyrat, F.; Ningthoujam, R. S.; Chakrabarti, P. K. Microwave Absorption and the Magnetic Hyperthermia Applications of $Li_{0.3}Zn_{0.3}Co_{0.1}Fe_{2.3}O_4$ Nanoparticles in Multiwalled Carbon Nanotube matrix. *ACS Appl. Mater. Interfaces* **2017**, *9*, 40831−40845.
(46) Kumar, P.; Singh, S.; Gupta, B. K. Future Prospects of Luminescent Nanomaterial-Based Security Inks: from Synthesis to Anti-counterfeiting Applications. *Nanoscale* **2016**, *8*, 14297−14340.
(47) Trinh, C. D.; Hau, P. T. P.; Dang, T. M. D.; Dang, C. M. Sonochemical Synthesis and Properties of YVO_4:Eu^{3+} Nanocrystals for Luminescent Security Ink Applications. *J. Chem.* **2019**, 5749702.
(48) You, M.; Zhong, J.; Hong, Y.; Duan, Z.; Lin, M.; Xu, F. Inkjet Printing of Upconversion Nanoparticles for Anti-Counterfeit Applications. *Nanoscale* **2015**, *7*, 4423−4431.
(49) Joshi, R.; Perala, R. S.; Shelar, S. B.; Ballal, A.; Singh, B. P.; Ningthoujam, R. S. Super Bright Red Upconversion in $NaErF_4$:0.5% Tm@$NaYF_4$:20%Yb Nanoparticles for Anti-Counterfeit and Bioimaging Applications. *ACS Appl. Mater. Interfaces* **2021**, *13*, 3481−3490.
(50) Acharya, R.; Swain, K. K.; Shinde, A. D.; Bhamra, N. S.; Chakrabarty, K.; Karhadkar, C. G.; Singh, T.; Rana, Y. S.; Pujari, P. K.; Shukla, D. K.; Reddy, A. V. R. Utilization of Pneumatic Carrier Facility of Dhruva Reactor for Trace Element Determination by Neutron Activation Analysis. *J. Radioanal. Nucl. Chem.* **2014**, *302*, 1525−1530.
(51) Mahan, M. M.; Doiron, A. L. Gold nanoparticles as X-Ray, CT, and Multimodal Imaging Contrast Agents: Formulation, Targeting, and Methodology. *J. Nanomater.* **2018**, 5837276.

https://doi.org/10.1021/acsomega.1c01572
ACS Omega 2021, 6, 19471−19483